ADVANCED FUNCTIONAL MATERIALS
www.afm-journal.de

Materials Views
www.MaterialsViews.com

Flexible, Multifunctional, Magnetically Actuated Nanocomposite Films

*Georgios A. Sotiriou, Christoph O. Blattmann, and Sotiris E. Pratsinis**

Filler nanoparticles greatly enhance the performance of polymers and minimize filler content in the resulting nanocomposites. At the same time, they challenge the manufacturing of such nanocomposites by filler agglomeration and non-uniform spatial distribution. Here, multifunctional nanocomposite films are made by capitalizing on flame-synthesis of ceramic or metal filler nanoparticles followed by rapid, in situ deposition on sacrificial substrates, resulting in a filler film with controlled porosity. The polymer is then spin-coated on the porous film that retained its stochastic but uniform structure, resulting in nanocomposites with homogeneous filler distribution and high filler-loading. By sequential repetition of this procedure, sophisticated, multilayer, free-standing, plasmonic- (Ag-Fe_2O_3) and phosphorescent-superparamagnetic (Y_2O_3:Eu^{3+}- Fe_2O_3) actuators are made by precisely tuning the polymer thickness between each functional nanostructured layer. These actuators are quite flexible, have fast response times, and exhibit superior superparamagnetism due to their high filler content and homogeneous spatial distribution.

1. Introduction

Polymer nanocomposites combine the desired functionalities of both host matrix and inorganic fillers in sensors,[1] optoelectronics,[2] artificial muscles,[3] optical components[4] to name a few applications. The addition of fillers enhances a certain property of the matrix such as increased Young's modulus[5] and thermal stability[6] or introduces new properties such as luminescence[7] and magnetism.[8] This class of materials is not new; polymer nanocomposites exist for years, with perhaps the most well-known ones being motor vehicle tires reinforced with nanostructured carbon-black, giving them their characteristic color and durability. The superior performance of these materials has prompted extensive research on synthesis of nanocomposites with unprecedented functionalities as well as for invention and development of methods for their optimal and efficient manufacturing.[9]

When dimensions of inorganic fillers are reduced to nanoscale, composite properties improve significantly and, typically, much less filler is needed to achieve superior performance.[10] For example, polymer/layered silicates nanocomposites are thermally more stable than pure polymer,[11] and the mechanical strength of silicone rubber improves progressively for smaller fillers.[5] The use, however, of nanosized fillers is accompanied by a challenge; such fillers are difficult to disperse homogeneously without forming agglomerated fillers[12] and leaving large, filler-free[9] domains in the polymer matrix.

Several ways have been suggested to overcome that. One can use surfactants and/or attach compatible functional groups to the surface of filler nanoparticles and subsequently mix them with polymer.[13,14] This however requires additional chemicals and processing steps. Another alternative is layer-by-layer (LbL) adsorption[15] where polymer and nanoparticles are in two oppositely charged solutions and the probe is immersed multiple times in them.[16] Then nanoparticles are distributed evenly over the surface, at the cost, however, of multiple processing steps to create composites of a certain thickness and the use of charged polymers.[15] Recently, the LbL deposition rate has been increased significantly by spraying the corresponding polymer solutions.[17]

An attractive functionality that can be readily induced to polymer composites by filler particles, is superparamagnetism.[18] Such composites are typically made by embedding superparamagnetic iron oxide nanoparticles in the polymers. The resulting nanocomposites have the polymer flexibility and can be actuated by an external magnetic field to have potential applications in biosensing (lab-on-a-chip),[14] controlled drug-release[19] and electromagnetic interference shields.[20] These applications, however, are hindered by inhomogeneous dispersion of nanoparticles in the polymer as large agglomerates are typically formed,[20–22] while large polymer areas are void of such nanoparticles.[13]

Here, homogeneous, multifunctional and multilayer nanocomposite films are made rapidly by flame synthesis of nanofillers, direct deposition[23] and in situ annealing[24] followed by polymer spin-coating. This technique allows for fabrication of free-standing multilayer films with tunable thickness and composition with sophisticated functionalities (e.g., superparamagnetic, plasmonic and phosphorescent) and surface smoothness at high filler-contents without large filler agglomerates or void patches. Furthermore, a variety of sophisticated filler nanoparticles[25] and host polymers can be employed, while this

Dr. G. A. Sotiriou, C. O. Blattmann, Prof. S. E. Pratsinis
Particle Technology Laboratory
Institute of Process Engineering
ETH Zurich, Sonneggstrasse 3
CH-8092 Zurich, Switzerland
E-mail: pratsinis@ptl.mavt.ethz.ch

DOI: 10.1002/adfm.201201371

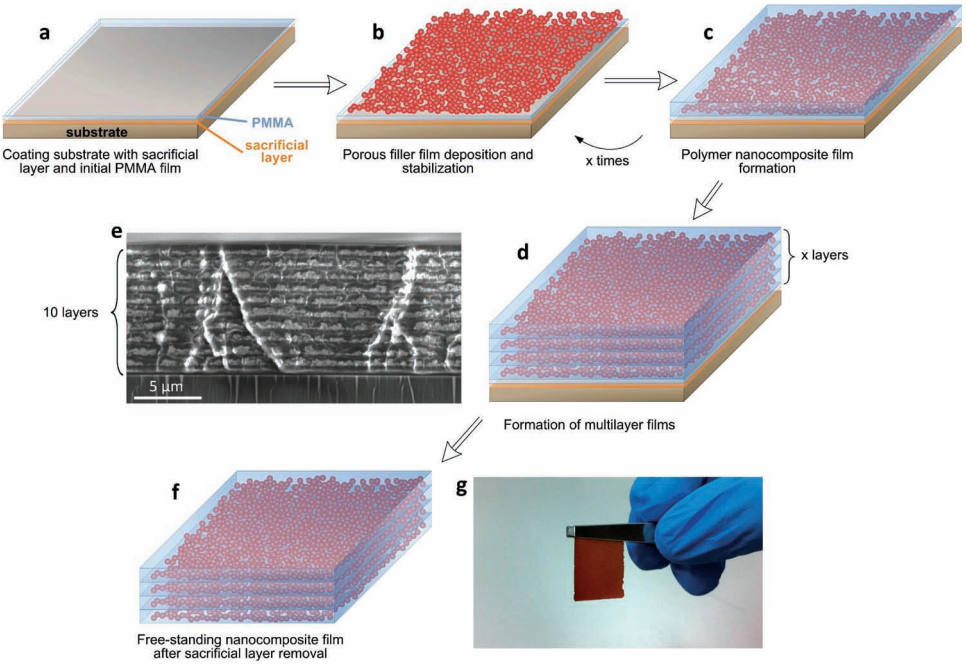

Figure 1. Nanocomposite film fabrication. a) Deposition of the sacrificial layer and an initial polymer film by spin-coating, b) subsequent particle film deposition and spin-coating of the polymer solution forming, thus, a homogeneous nanocomposite film (c). This process can be repeated (e.g., *x* times) to form multilayer films (d,e). Upon removal of the sacrificial layer, free-standing nanocomposite films can be made (f,g).

technique is fast, highly reproducible and scalable[26] that may facilitate commercialization of such nanocomposites.

2. Results and Discussion

2.1. Multilayer Nanocomposite Fabrication

The nanocomposite fabrication sequence is shown in **Figure 1**a. Initially, a thin polymer film (e.g., PMMA) is deposited by spin-coating on a substrate (e.g., silicon, metal, glass). The initial polymer film thickness is selected by the spin-coating speed and the polymer solution viscosity. A nanoparticle filler layer is then deposited[23] on that polymer film and in situ annealed and stabilized[24] (Figure 1b). With this last step the film porosity can be reduced[24] from 98% to about 60% facilitating the embedding of high filler contents in the nanocomposite. Additional polymer solution is spin-coated on top of that stabilized filler layer filling its voids (Figure 1c). By selecting again the spin-coating conditions, the composite thickness is controlled. By repeating nanoparticle deposition and polymer spin-coating, multiple layers can be made with controlled filler composition and structure (Figure 1d,e). It should be noted that flame-synthesis allows for a wide selection of nanoparticles and morphologies[25] broadening, therefore, the potential target applications of such inorganic/polymer nanocomposites. Hence, by choosing appropriate precursors,[25] multilayer and multifunctional polymer nanocomposites (e.g., magnetic-plasmonic, magnetic-phosphorescent) are made.

A key advantage of the current process is the synthesis of free-standing nanocomposite films. This is achieved by depositing first a sacrificial layer on the substrate. Then the nanocomposite can be released resulting in a free-standing multifunctional film having a thickness from tens of nanometers to a few micrometers (Figure 1f,g). This indicates the compatibility of this process with existing techniques for fabrication of magnetic cantilevers that are integrated in microelectromechanical systems (MEMS) for biosensing.[14] The present technique, however, offers several advantages: i) there is a broad selection of inorganic filler materials that can be readily used (e.g., no charging is needed), ii) it involves few process steps since nanoparticle synthesis and deposition occurs in a single-step,[24] iii) there is practically no limitation on chosen polymers, iv) relatively thick films (e.g., 1–10 µm) can be made also, and finally v) it is scalable and CMOS wafer-level compatible.[24]

2.2. Nanostructured Particle Film Deposition

The nanoparticle film thickness corresponds to its coating density[27] on the substrates for a given film porosity, and is shown in **Figure 2**a as a function of deposition time. The main crystal phase of the flame-made[28] and directly-deposited Fe_2O_3 nanoparticles is maghemite (γ-Fe_2O_3) with an average crystal size of about 9.4 nm and primary particle size of 9.9 nm (by N_2 adsorption, Supporting Information, Figure S1a), indicating rather monocrystalline iron oxide nanoparticles. Similar flame-made Fe_2O_3 nanoparticles have a log-normal particle size distribution with geometric standard deviation[28] σ_g = 1.36–1.52, typical for nanoparticles grown by coagulation and sintering.[25] Such Fe_2O_3 nanoparticles are superparamagnetic at room temperature[28] with a saturation magnetization of M_s = 37 emu/g

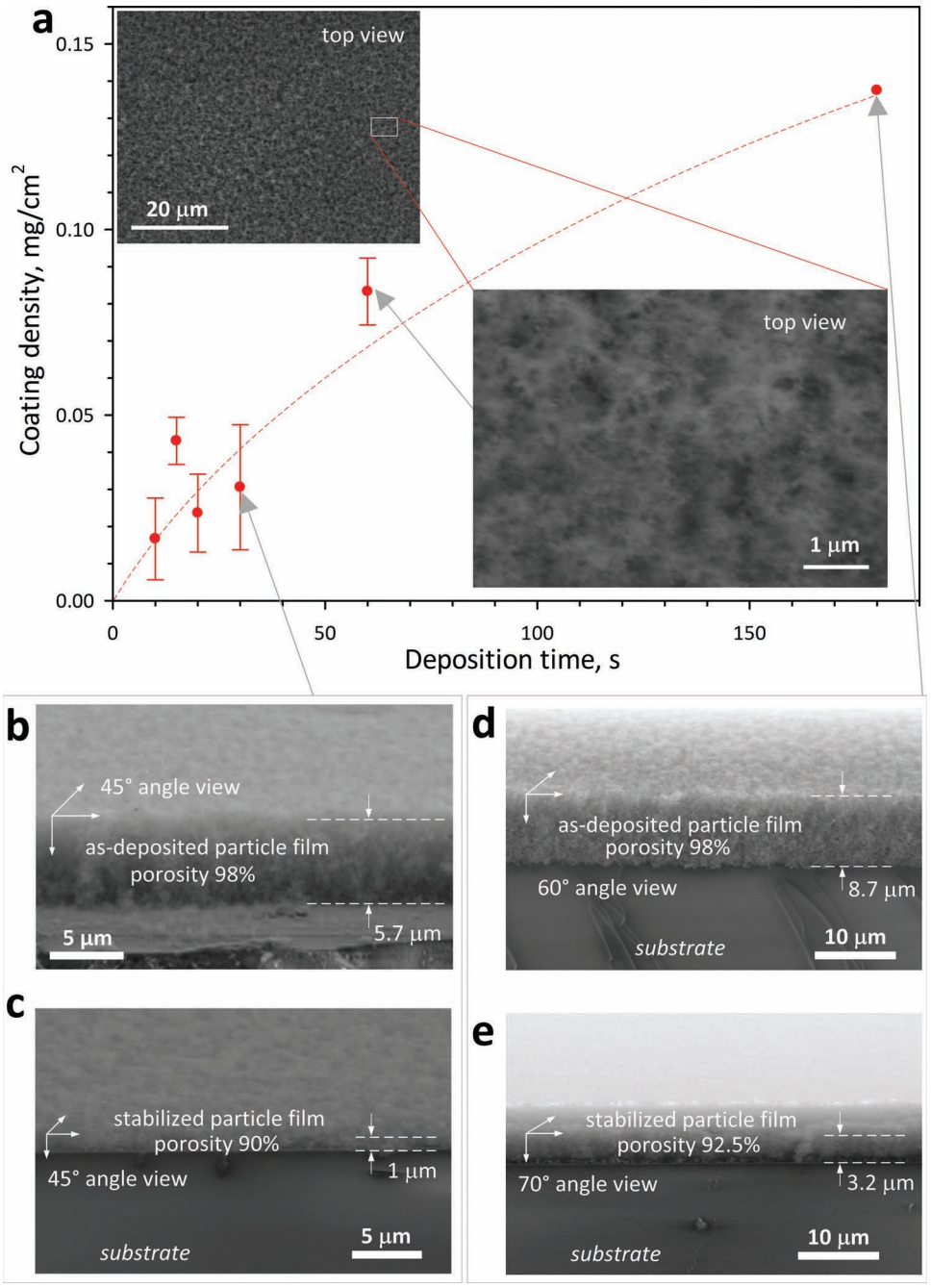

Figure 2. Particle filler-film deposition and stabilization. a) The filler-film coating density (equivalent to film thickness for a given porosity) can be finely tuned by the deposition time. SEM images of such particle filler-films (at various angles) for 30 (b,c) and 180 s (d,e) before (b,d) and after (c,e) their mechanical stabilization (in situ annealing). The insets in (a) shows two SEM images (top view) of an as-deposited film for 60 s.

(Supporting Information, Figure S1c). The insets of Figure 2a show two top-view SEM images of a Fe_2O_3 particle film. For both magnifications the particle film is highly homogeneous clearly showing that the filler film is finely distributed on the PMMA polymer layer (Figure 1a) without any large agglomerates. Figure 2 shows also scanning emission microscope (SEM) images of nanoparticle films at various angles (45–70°) for deposition of 30 (b,c) and 180 s (d,e). The as-prepared films (Figure 2b,d) are highly porous, about 98%, as typically obtained by flame aerosol deposition.[23] As expected, the coating density or film thickness increases with prolonged deposition allowing therefore, the fine-tuning of the nanoparticle film thickness. After in situ stabilization (Figure 2c,e), however, the particle films are compacted regardless of deposition time, decreasing therefore their porosity to ≈90%. This stabilization through in situ annealing, however, does not influence the primary particle size. This is crucial as larger iron oxide nanoparticles lose their superparamagnetism.

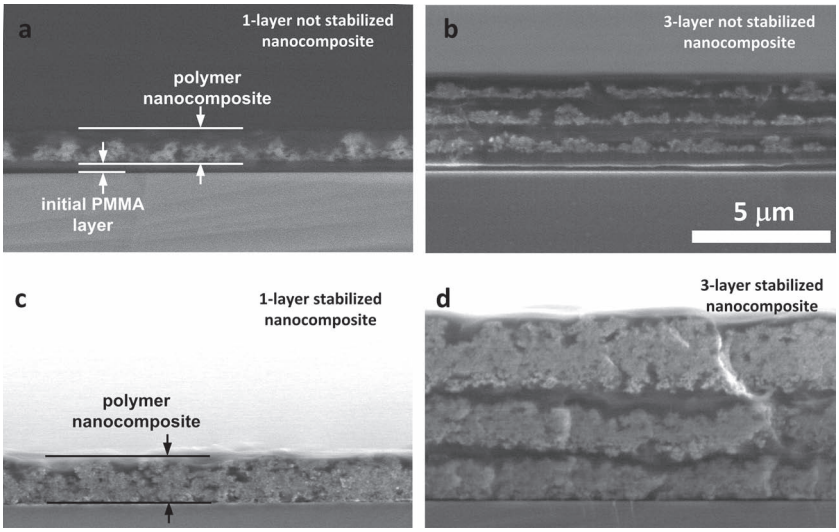

Figure 3. SEM cross-sectional images of Fe_2O_3/PMMA nanocomposites containing a 1-layer (a,c) and 3-layer (b,d) non-stabilized (a,b) and stabilized (c,d) Fe_2O_3 films. the scale bar is identical for all images.

2.3. Polymer Nanocomposite Synthesis

After spin-coating of the polymer solution on an as-deposited (without stabilization) nanorough Fe_2O_3 particle film (as in Figure 2b,d), a nanocomposite film can be made. **Figure 3**a shows a cross-sectional SEM image of such a nanocomposite film. The viscous forces of the polymer solution during spin-coating are strong enough to collapse any loosely-connected, as-deposited nanostructured film. This forms a vertically rather inhomogeneous nanocomposite, as there are areas with large agglomerates. Even though the particle film collapses, the homogeneity in the horizontal plane is retained (Supporting Information, Figure S2). In fact, by repeating polymer solution spin-coating and particle deposition, multilayer films can be made by precisely tuning the distance (or polymer thickness) between filler nanoparticle films (Figure 3b).

When, however, the as-deposited particle films are stabilized by in situ annealing (Figure 2c) prior to spin-coating, no structural changes occur to these films during polymer deposition (Figure 3c). This is attributed to the higher adhesion and cohesion of the stabilized films,[24] enabling them to withstand the viscous forces during polymer spin-coating. Furthermore, one major difference between "as-deposited" and "stabilized" particle films is their porosity and consequently the filler-loading of the resulting nanocomposites. The lower porosity of the stabilized film enables nanocomposites to obtain theoretical high loadings up to 30–40 vol%[24] but still preserving their homogeneity without the need of any filler surface-functionalization.[14,29] In fact, high filler-loadings (up to 12 vol%) can improve significantly the mechanical strength of nanocomposites and broaden their applications, as it has been shown recently with silica nanoparticles in silicone rubber.[5] This is a major advantage of the present technique, as it overcomes nanoparticle agglomeration that typically increases with filler loadings above a few vol%.[15,29] The surface of as-prepared flame-made nanoparticles is typically hydrophilic[30] hindering their easy dispersion in typically hydrophobic polymers.[10] The present technique, however, enables synthesis of such nanocomposites that exhibit indeed superior filler-specific functionality (e.g., high magnetization) without compromising film homogeneity and surface smoothness.[29] Figure 3d shows a cross-sectional SEM image of a three-layer iron oxide/PMMA nanocomposite. The stabilized dense particle films are completely embedded in the PMMA and are separated by a tunable spacing by adjusting the polymer spin-coating speed. Such layered structures could incorporate multiple film functionalities by selecting the filler composition as it is shown below. It should be noted that there are no separate inorganic filler domains within the polymer film as typically seen with nanocomposites made by solvent-melt blending (Supporting Information, Figure S3) but rather a homogeneous and continuous layer is deposited that maintains its structure during and after polymer addition (Figure 3).

2.4. Superparamagnetic Nanocomposite Actuator Films

The magnetic performance of these nanocomposites is investigated by monitoring their magnetization. **Figure 4**a shows the magnetization of three iron oxide/PMMA nanocomposites: a 3-layer one with its filler particle film as-prepared (or not stabilized, green line), as well as 1-layer (red line) and 3-layer (blue line) nanocomposites with stabilized particle films by in situ annealing. The 1-layer nanocomposite film has the highest magnetization (M_s = 6.4 emu/g of nanocomposite), which is almost thrice higher than that of nanocomposite films made by solvent-melt blending[14,20,21] (Supporting Information, Figure S3). This is one of the highest reported M_s for a composite with homogeneous inorganic filler distribution and controlled surface smoothness compatible with M/NEMS fabrication techniques. This exceptionally high magnetization is attributed to its uniform, high filler-loading (35 wt% or 10 vol% determined thermogravimetrically).

The 3-layer stabilized nanocomposite (Figure 4, blue line) has M_s = 4.5 emu/g of nanocomposite. This lower magnetization is attributed largely to the lower filler-loading (increased polymer present between particle layers) than the 1-layer nanocomposite (red line). The filler-loading of this sample is ≈30 wt% (9 vol%), as the interlayer distance was kept minimal. It should be noted that the measured filler-loadings vol% correspond quite well to the porosity of the stabilized particle films calculated in Figure 2 accounting also for the polymer layer between filler layers. This indicates that indeed the polymer solution fills the pores of the stabilized nanoparticle film. However, the M_s of the 3-layer nanocomposite containing the loosely-connected (non-stabilized) and, as a result, non-uniform iron oxide particle film (green line) is significantly lower (M_s = 2.6 emu/g) than that of nanocomposites with stabilized filler particle films. The lower magnetization of this film is

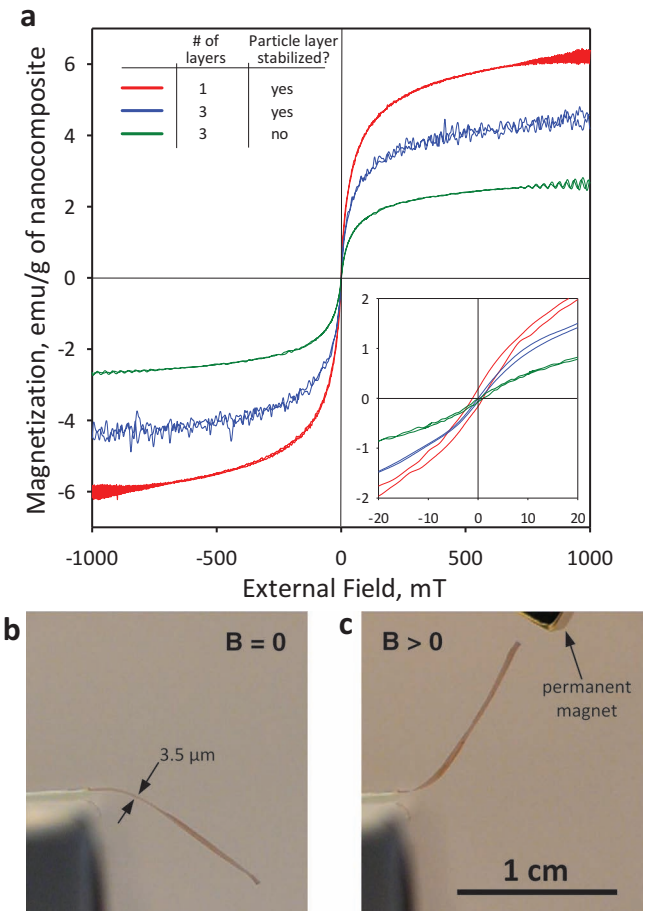

Figure 4. Superparamagnetic Fe_2O_3/PMMA films. a) Magnetization of polymer nanocomposites consisting of a 1-layer (red line) and 3-layer (blue line) stabilized and 3-layer non stabilized (green line) particle filler-films. The highest magnetization achieved is 6.4 emu/g of composite for the 1-layer stabilized particle filler-film. This free-standing, 3.5 µm thin, nanocomposite film can be actuated by an external magnetic field as shown in (b,c).

attributed mostly to its lower filler-loading of 20 wt% (5.3 vol%) as there is much more polymer there. This clearly shows the advantage of in situ stabilization that helps the inorganic films to retain their homogeneity during spin-coating and leads to synthesis of high magnetization nanocomposites suitable for bioapplications.[14,19]

The present nanocomposites are superparamagnetic since there is no significant hysteresis in their M_s (Figure 4a, inset). This indicates that particles have retained their superparamagnetism (Supporting Information, Figure S1b) after polymer spin-coating and, therefore, can be actuated by a magnetic field. The magnetic response of the stabilize 1-layer nanocomposite film that exhibited the highest M_s (red line) is shown in Figure 4 in the absence (b, B = 0) and presence (c, B > 0) of a magnetic field. Clearly, when a permanent magnet is approached, this 3.5 µm thin nanocomposite cantilever is actuated with a fast response time (see Supporting Information for a video). This shows the flexibility of the present nanocomposite films).

2.5. Plasmonic-and Luminescent-Superparamagnetic Actuators

After formation of the superparamagnetic nanocomposite layer, additional particle films can be deposited consisting of another material, such as plasmonic nanosilver,[31] followed again by polymer spin-coating. **Figure 5**a shows a cross-sectional SEM image of such a nanocomposite film consisting of a stabilized iron oxide particle film on the bottom and a second layer on top with Ag/SiO_2 nanoparticles[32] (50 wt% Ag, d_{Ag} = 9 nm), spaced by a PMMA film with controllable thickness. Silver appears brighter in SEM because of its higher proton-number than iron. This clearly shows that the particle film homogeneity is retained also for other materials than iron oxide.

The magnetic behavior of this hybrid actuator is shown in Figure 5b. This nanocomposite retains the superparamagnetic performance of the iron oxide nanoparticles, as there is no magnetization hysteresis (Figure 5b, inset). The maximum magnetization is M_s = 2.4 emu/g which is lower than the 1-layer iron oxide/PMMA nanocomposite (Figure 4a, red line) due to the presence of magnetically inactive Ag/SiO_2. Such M_s, however, is comparable to that achieved by other nanocomposites containing only iron oxide nanoparticles.[14]

The presence of plasmonic silver nanoparticles enables this hybrid[33] nanocomposite to be employed in biosensing[34] and optoelectronics.[4,35,36] Figure 5c shows the extinction spectra of a 1-layer stabilized superparamagnetic (red line) and a hybrid superparamagnetic-plasmonic (blue line) nanocomposite. The latter exhibits a strong plasmon peak around 400 nm, characteristic for silver nanoparticles.[31,37] Such a multifunctional actuator could be integrated in "smart" lab-on-a-chip[14] M/NEMS biosensors with controlled drug-release.

Phosphorescent-superparamagnetic films can be made also using this technique. So **Figure 6**a shows an image of a 2-layer nanocomposite consisting of an iron oxide film followed by a phosphorescent film of yttrium oxide particles doped with 8 at% europium.[27] These Y_2O_3:Eu^{3+} particles are mostly cubic with an average primary particle size of 24 nm.[27] After initial iron oxide deposition and stabilization (initial 1 µm), phosphorescent film deposition followed (next 1.7 µm) with minimal polymer film between the two fillers (<100 nm, not detectable by SEM in Figure 6a). Again the higher proton-number yttrium makes the Y_2O_3:Eu^{3+} film brighter than the iron oxide one. After deposition of the second filler, the polymer solution was deposited by spin-coating resulting in the final hybrid phosphorescent-superparamagnetic nanocomposite with an excess PMMA of 0.5 µm.

Figure 6b shows the phosphorescent emission spectra of an as-prepared Fe_2O_3/Y_2O_3:Eu^{3+} film (blue solid line, no PMMA) and of a Fe_2O_3/Y_2O_3:Eu^{3+}/PMMA nanocomposite (red broken line) for excitation irradiation at 254 nm. The characteristic emission peak at 612 nm attributed to the Eu^{3+} ion transitions is present in both materials. The emission intensity is slightly higher for the Y_2O_3:Eu^{3+} particle film than its polymer nanocomposite. This is attributed to (UV-light) absorption of the excitation irradiation by the PMMA film,[38] and therefore the Eu^{3+} ions in the nanocomposite are excited with less power. The emission color of such nanocomposites can be finely tuned from blue to red by controlling the Y_2O_3 doping composition

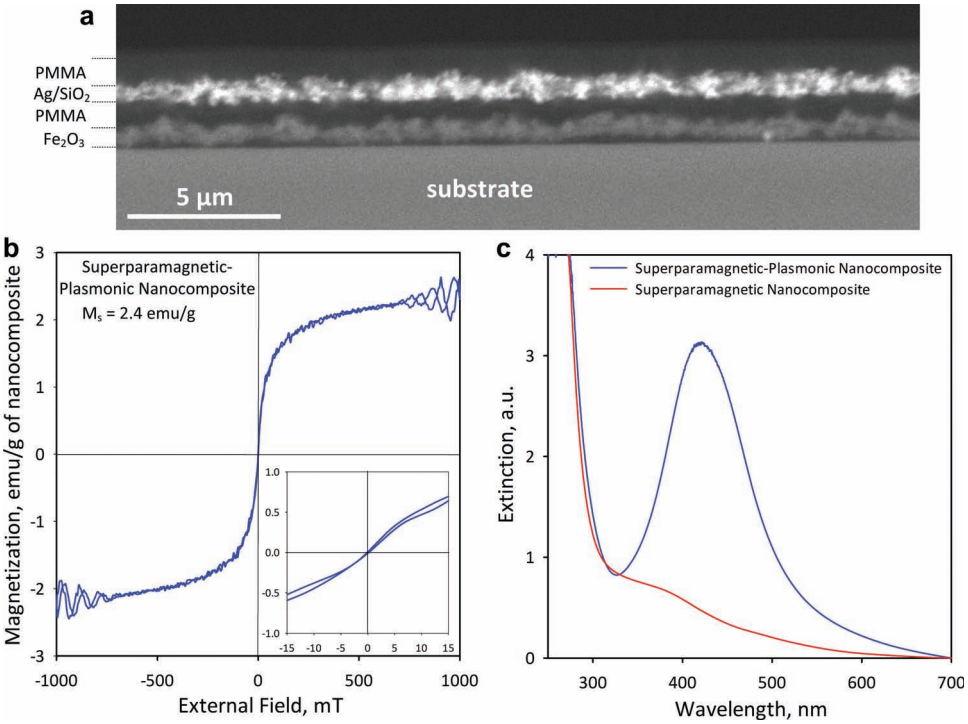

Figure 5. Multilayer plasmonic-superparamagnetic nanocomposite film. a) SEM cross-sectional image of a polymer nanocomposite film consisting of a grey superparamagnetic (Fe_2O_3) and a bright plasmonic (Ag/SiO_2) particle filler-film. The plasmonic film is brightest because of the highest proton-number Ag. The two inorganic layers are separated by a dark PMMA film, which can be finely tuned by the spin-coating conditions. This multilayer nanocomposite (blue line) exhibits both superparamagnetic (b) and plasmonic (c) properties of its two inorganic components.

with Tb^{3+} and Eu^{3+} ions during their flame-synthesis.[39] This hybrid nanocomposite can also be actuated in the presence of an external magnetic field (Figure 6c,d) while simultaneously exhibiting its characteristic phosphorescence when excited with UV irradiation (254 nm, Figure 6e). These attractive photoluminescent properties enable the present nanocomposites to be implemented in biological detection[40] and simultaneous magnetic manipulation.

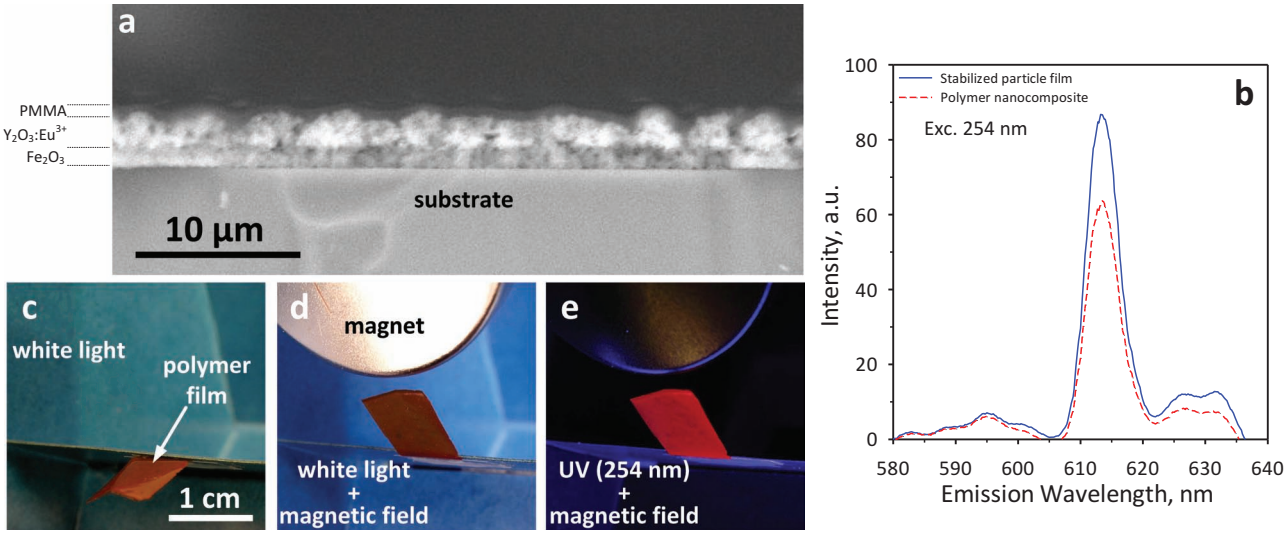

Figure 6. Multifunctional phosphorescent-superparamagnetic polymer nanocomposite film. a) SEM cross-sectional image of that film consisting of a superparamagnetic Fe_2O_3 and a phosphorescent $Y_2O_3:Eu^{3+}$ particle filler film, embedded in PMMA. b) The phosphorescence of the pure $Y_2O_3:Eu^{3+}$ (8 at%) particle film (blue solid line) and its corresponding nanocomposite film (red broken line) for excitation at 254 nm show the characteristic red emission attributed to the Eu^{3+} ion transitions. This multifunctional nanocomposite exhibits also both superparamagnetic (c,d) and phosphorescent (d,e) properties from its two inorganic components.

3. Conclusions

Multilayer and flexible polymer nanocomposite actuators with multiple functionalities were made by a scalable technique. Most importantly, by capitalizing on versatile flame synthesis of nanoparticles and their direct deposition and stabilization on substrates, layered nanocomposites with high filler-loadings with excellent homogeneity were created. That way superparamagnetic iron oxide nanoparticles of about 10 nm in diameter were embedded in PMMA. By controlling the particle film deposition and adhesion/cohesion, high filler loadings were achieved with spatial uniformity resulting in high nanocomposite magnetization and fast response in a magnetic field. By repeating sequentially the nanocomposite fabrication procedure, multilayer films with multiple functionalities were created. So flexible plasmonic-superparamagnetic and phosphorescent-superparamagnetic nanocomposite actuators were made that could be employed in biosensing including M/NEMS, controlled drug-release and luminescent immunoassays.

4. Experimental Section

Particle Synthesis and Film Deposition: Maghemite (γ-Fe_2O_3) nanoparticles were formed by flame spray pyrolysis with a precursor solution of 0.34 M Fe^{3+} from iron(III)acetylacetonate (Fluka, powder, >97%) dissolved in 3:1 xylene (Sigma-Aldrich) to acetonitrile (Sigma-Aldrich, >99.5%). The precursor solution was fed through the burner capillary by a syringe pump (InoTech) at a rate of 5 mL min^{-1}, dispersed by O_2 (5 L min^{-1}, PanGas 3.5) and ignited by a supporting flame of CH_4 (1.5 L min^{-1}, PanGas 2.5) and O_2 (3.2 L min^{-1}).[23] The feed rates of all gases to the nozzle were regulated with a Bronkhorst HI-TEC E7100-DDD flow controller. Phosphorescent nanoparticles were made dissolving 0.5 M yttrium hexanitrate anhydrate (Aldrich, >99.9%) in a solution of 1:1 ethanol (EtOH, Alcosuisse, 3, II) to 2-ethylhexanoc acid (2-EHA, Aldrich) doped with 8 at% with europium pentanitrate hydrate (Fluka, 95%). The precursor solution was fed at 11.3 L min^{-1} through the capillary and dispersed by 3 L min^{-1} O_2.[39] Silver-silica nanoparticles (50 wt% Ag)[32] were made by dissolving silver acetate (Sigma Aldrich, >99.0%) in 1:1 2-EHA to acetonitrile and stirred in an oil bath at 110 °C for 1 h. After the solution was cooled to room temperature, hexamethyldisiloxane (HMDSO, Fluka, >98.5%) was added. The total metal ion concentration was 1.35 M. This precursor solution was fed into the flame at 5 mL min^{-1} and dispersed by 5 L min^{-1} of O_2. For all particle syntheses the nozzle and capillary were water-cooled and 5 L min^{-1} of O_2 as a sheath gas was applied. The nozzle pressure drop was set to 1.5 bar. As-prepared nanoparticles were collected onto a glass microfiber filter (Whatman) located above the flame (≈50 cm) with the aid of a vacuum pump.[23]

Particle film deposition was done from 5 s to 5 min onto a silicon or glass substrate 20 cm above and at crossflow to the flame.[23] The substrate was cooled throughout the process. Before deposition, substrates were cleaned with ethanol and dried with pressurized air. For polymer nanocomposite fabrication, substrates were coated additionally with a layer of poly(methyl methacrylate) (PMMA, Sigma Aldrich) by spin-coating (Laurell, WS-650MZ-NPP/LITE) a 10 wt% solution of PMMA in anisole (Fluka Analytical, >99%). The solution (≈0.25 mL) was deposited onto the substrate and spun with an acceleration of +100 rpm s^{-1} to 500 rpm for 5 s and following at +1000 rpm s^{-1} to 3000-4850 rpm for 45 s. By placing the substrate onto a hot plate (VWR VHP-C7) at 180 °C for ≈2 min the remaining anisole was allowed to evaporate. For the fabrication of a free-standing or removable polymer nanocomposite films, the substrate was first coated with a sacrificial layer by depositing PMGI SF 9 (≈0.3 mL, MicroChem) onto the cleaned substrate and spin-coating up to 3000 rpm. The substrate was then dried on a hot plate at 180 °C for >5 min before proceeding with the addition of the PMMA layer. In situ direct flame annealing[24] was done by exposing the particle film to a particle-free xylene flame and sheath gas, as during particle synthesis. The xylene flow rate ranged from 9 to 12 mL min^{-1} and dispersed with 5 L min^{-1} with O_2. The substrate was located at 20 cm above the nozzle and water-cooled throughout the in situ annealing.

Polymer Nanocomposite Synthesis: A polymer nanocomposite was created by spin-coating a 10 wt% PMMA in anisole solution onto a particle film. The spin-coating settings used were identical to those applied for the above substrate coating with a maximum end-rotation speed of 1000–4850 rpm. The embedded particle film was not always annealed prior to spin-coating. Multiple layered polymer nanocomposites were achieved by depositing additional particle films onto the existing nanocomposite structure. Each particle film was mechanically stabilized, if necessary, by in situ flame annealing and spin-coated with the PMMA solution. To create multifunctional polymer nanocomposites, this technique was applied, while depositing particle films consisting of different materials.

To remove a polymer nanocomposite film from the substrate with a sacrificial layer, the substrate with film was fully submersed in Microposit 351 Developer (Shipley Company). After >24 h the film could be easily removed with tweezers and washed with ethanol and water.

For comparison, polymer nanocomposites were also created by solvent melt blending. Flame-made nanoparticles collected from a filter[13] were dispersed in a 10 wt% PMMA in anisole solution by sonication for 5 min at 75% power, 0.5/0.5 pulse on/off (Merck Sonics Vibra Cell). Additionally, surfactant MEMO (MPS, 3-(trimethoxysilyl) propyl methacrylate, Fluka, >98%) was added to the solution before sonication at a concentration of 8 molecules of surfactant per nm^2 of nanoparticle.[13] The sonicated solution was spin-coated onto clean glass substrates at the same conditions applied earlier for the pure PMMA solution at a maximum rotation speed ranging from 1700 to 4000 rpm. The film was allowed to dry on a hot plate at 180 °C for >2 min.

Particle Characterization: Particles collected on the filter were analyzed by X-ray diffraction (Bruker AXS D8 advance, 40 kV, 40 mA, Cu Kα radiation) for a range of 2θ = 15–70° in interval steps of 0.03°. The received data graphs were analyzed with the software Topas4. The specific surface area and primary particle diameter were obtained by N_2 adsorption (Micromeritics TriStar at 77K). All samples were degassed for at least 1 h at 150 °C. High-resolution transmission electron microscopy was performed with a CM30ST microscope (FEI; LaB6 cathode, operated at 300 kV, point resolution ≈2 Å). The electron beam could be set to selected areas to determine material composition by energy dispersive X-ray spectroscopy. Product particles were dispersed in ethanol and deposited onto a perforated carbon foil supported on a copper grid. The magnetization analysis was done in a MicroMag 3900 VSM (vibrating sample magnetometer) at 300 K.

Particle and Polymer Film Characterization: Substrates were weighed before and after particle deposition (Mettler Toledo AB135-S/FACT, 0.01 mg) to determine the accumulated film weight. The calculated values were confirmed with scanning electron microscope image analysis (FEI Quanta 200 FEG or Hitachi TM-1000 Table Microscope) in the SE and BSE mode at 40 Pa and 5–15 kV. The film homogeneity was analyzed with a light microscope (Zeiss AXIO Imager.M2m) in the transmitted light mode for glass substrates and reflected light mode for silicon substrates at magnifications up to 100X.

Polymer nanocomposites were analyzed by light microscope (as above) images of the film horizontal plane and SEM (as above) images of the film cross-sections. Magnetization measurements of the nanocomposite films were made after their release from the substrate as described above. The phosphorescence was measured by a Varian Cary Eclipse spectrophotometer containing a Xe flash lamp with tunable emission wavelength. The optical extinction spectra were obtained with a Varian Cary 500 spectrophotometer. The filler content of the nanocomposite was measured by thermogravimetric analysis (TGA, Netzsch Jupiter STA 449C) in the TGA-DSC mode. The nanocomposite was either scratched off the substrate with a razor blade or, if possible, by removing the sacrificial layer. The TGA chamber temperature was increased from 20 °C to 650 °C at +10 °C min^{-1} with constant argon

(PanGas 5.0) flow rate of 50 mL min^{-1}. The composition of the burnt off-gases was analyzed with a mass spectrometer (Netzsch Aëolos QMS 403 C).

Supporting Information

Supporting Information is available from the Wiley Online Library or from the author.

Acknowledgements

The authors thank Dr. Frank Krumeich (Electron Microscopy Center, ETH Zurich) for the electron microscopy analysis. Financial support by the Swiss National Science Foundation (No. 200020-126694) and European Research Council are kindly acknowledged.

Received: May 21, 2012
Revised: July 13, 2012
Published online: August 8, 2012

[1] C. Hagleitner, A. Hierlemann, D. Lange, A. Kummer, N. Kerness, O. Brand, H. Baltes, *Nature* **2001**, *414*, 293.
[2] S. A. McDonald, G. Konstantatos, S. G. Zhang, P. W. Cyr, E. J. D. Klem, L. Levina, E. H. Sargent, *Nat. Mater.* **2005**, *4*, 138.
[3] Z. M. Dang, L. Wang, Y. Yin, Q. Zhang, Q. Q. Lei, *Adv. Mater.* **2007**, *19*, 852.
[4] W. Caseri, *Chem. Eng. Commun.* **2009**, *196*, 549.
[5] A. Camenzind, T. Schweizer, M. Sztucki, S. E. Pratsinis, *Polymer* **2010**, *51*, 1796.
[6] T. Kashiwagi, F. M. Du, J. F. Douglas, K. I. Winey, R. H. Harris, J. R. Shields, *Nat. Mater.* **2005**, *4*, 928.
[7] F. N. Sayed, V. Grover, K. A. Dubey, V. Sudarsan, A. K. Tyagi, *J. Colloid. Interface Sci.* **2011**, *353*, 445.
[8] A. H. Lu, E. L. Salabas, F. Schuth, *Angew. Chem. Int. Ed.* **2007**, *46*, 1222.
[9] T. E. Twardowski, *Introduction to Nanocomposite Materials: Properties, Processing, Characterization*, DEStech Publications, Inc., Lancaster, PA **2007**.
[10] A. Camenzind, W. R. Caseri, S. E. Pratsinis, *Nano Today* **2010**, *5*, 48.
[11] K. Chrissopoulou, I. Altintzi, I. Andrianaki, R. Shemesh, H. Retsos, E. P. Giannelis, S. H. Anastasiadis, *J. Polym. Sci. Part. B: Polym. Phys.* **2008**, *46*, 2683.
[12] H. Schulz, B. Schimmoeller, S. E. Pratsinis, U. Salz, T. Bock, *J. Dent.* **2008**, *36*, 579.
[13] H. Schulz, S. E. Pratsinis, H. Rugger, J. Zimmermann, S. Klapdohr, U. Salz, *Colloids Surf. A* **2008**, *315*, 79.
[14] M. Suter, O. Ergeneman, J. Zürcher, C. Moitzi, S. Pané, T. Rudin, S. E. Pratsinis, B. J. Nelson, C. Hierold, *Sens. Actuators B* **2011**, *156*, 433.
[15] S. Srivastava, N. A. Kotov, *Acc. Chem. Res.* **2008**, *41*, 1831.
[16] F. Hua, T. Cui, Y. M. Lvov, *Nano Lett.* **2004**, *4*, 823.
[17] K. C. Krogman, J. L. Lowery, N. S. Zacharia, G. C. Rutledge, P. T. Hammond, *Nat. Mater.* **2009**, *8*, 512.
[18] J. K. Oh, J. M. Park, *Progr. Polym. Sci.* **2011**, *36*, 168.
[19] T. Hoare, B. P. Timko, J. Santamaria, G. F. Goya, S. Irusta, S. Lau, C. F. Stefanescu, D. B. Lin, R. Langer, D. S. Kohane, *Nano Lett.* **2011**, *11*, 1395.
[20] J. Gass, P. Poddar, J. Almand, S. Srinath, H. Srikanth, *Adv. Funct. Mater.* **2006**, *16*, 71.
[21] M. Suter, O. Ergeneman, J. Zürcher, S. Schmid, A. Camenzind, B. J. Nelson, C. Hierold, *J. Micromech. Microeng.* **2011**, *21*, 025023.
[22] S. Gyergyek, M. Huskic, D. Makovec, M. Drofenik, *Compos. Interfaces* **2010**, *17*, 137.
[23] L. Madler, A. Roessler, S. E. Pratsinis, T. Sahm, A. Gurlo, N. Barsan, U. Weimar, *Sens. Actuators B* **2006**, *114*, 283.
[24] A. Tricoli, M. Graf, F. Mayer, S. Kuhne, A. Hierlemann, S. E. Pratsinis, *Adv. Mater.* **2008**, *20*, 3005.
[25] R. Strobel, S. E. Pratsinis, *J. Mater. Chem.* **2007**, *17*, 4743.
[26] S. E. Pratsinis, *AIChE J.* **2010**, *56*, 3028.
[27] R. Kubrin, A. Tricoli, A. Camenzind, S. E. Pratsinis, W. Bauhofer, *Nanotechnology* **2010**, *21*, 225603.
[28] D. Li, W. Y. Teoh, C. Selomulya, R. C. Woodward, R. Amal, B. Rosche, *Chem. Mater.* **2006**, *18*, 6403.
[29] S. Taccola, A. Desii, V. Pensabene, T. Fujie, A. Saito, S. Takeoka, P. Dario, A. Menciassi, V. Mattoli, *Langmuir* **2011**, *27*, 5589.
[30] R. Mueller, H. K. Kammler, K. Wegner, S. E. Pratsinis, *Langmuir* **2002**, *19*, 160.
[31] G. A. Sotiriou, T. Sannomiya, A. Teleki, F. Krumeich, J. Vörös, S. E. Pratsinis, *Adv. Funct. Mater.* **2010**, *20*, 4250.
[32] G. A. Sotiriou, S. E. Pratsinis, *Environ. Sci. Technol.* **2010**, *44*, 5649.
[33] G. A. Sotiriou, A. M. Hirt, P. Y. Lozach, A. Teleki, F. Krumeich, S. E. Pratsinis, *Chem. Mater.* **2011**, *23*, 1985.
[34] G. A. Sotiriou, S. E. Pratsinis, *Curr. Opin. Chem. Eng.* **2011**, *1*, 3.
[35] F. Faupel, V. Zaporojtchenko, T. Strunskus, M. Elbahri, *Adv. Eng. Mater.* **2010**, *12*, 1177.
[36] S. Malynych, H. Robuck, G. Chumanov, *Nano Lett.* **2001**, *1*, 647.
[37] D. D. Evanoff, G. Chumanov, *ChemPhysChem* **2005**, *6*, 1221.
[38] D. Koziej, F. Fischer, N. Kränzlin, W. R. Caseri, M. Niederberger, *ACS Appl. Mater. Interfaces* **2009**, *1*, 1097.
[39] G. A. Sotiriou, M. Schneider, S. E. Pratsinis, *J. Phys. Chem. C* **2011**, *115*, 1084.
[40] L. Y. Wang, R. X. Yan, Z. Y. Hao, L. Wang, J. H. Zeng, H. Bao, X. Wang, Q. Peng, Y. D. Li, *Angew. Chem. Int. Ed.* **2005**, *44*, 6054.